HIGHER ORDER FINITE ELEMENT METHOD FOR INHOMOGENEOUS AXISYMMETRIC RESONATORS

X. Rui [†] and J. Hu

School of Electronic Engineering
University of Electronic Science and Technology of China
Chengdu, Sichuan 610054, China

Q. H. Liu

Department of Electrical and Computer Engineering
Duke University
Durham, NC 27708, USA

Abstract—To analyze resonances in an axisymmetric inhomogeneous cavity, a higher-order finite element method (FEM) is developed. Mixed higher-order node-based and edge-based elements are applied to eigenvalue analysis for the azimuthal component and meridian components of the field, respectively. Compared with the lower-order FEM, the higher-order FEM can improve accuracy with the same number of unknowns and can reduce the CPU time and memory requirement for specified accuracy. Numerical results are given to demonstrate the validity and efficiency of the proposed method.

1. INTRODUCTION

Electromagnetic computation for bodies of revolution (BOR) of arbitrary shape has been widely discussed for many years. BOR objects of various types, including perfect electric conductors (PEC), homogeneous dielectric bodies, coated conducting bodies, combined dielectric and conducting bodies, multi-layer dielectric bodies and resonators with axial symmetry, have been studied [1–14]. Because of the axis-symmetry of the geometry, only the 2-D cross section that forms the volume (i.e., the meridian plane) is needed for solving the

---

Corresponding author: Q. H. Liu (qhliu@ee.duke.edu).
[†] Also with Department of Electrical and Computer Engineering, Duke University, Durham, NC 27708, USA

scattering, radiation and resonance problems of the BOR by integral equations (IE) [1–5], finite element method (FEM) [12–14], hybrid finite element method and boundary integration (FEM-BI) [15], hybrid physical optics and method of moments (PO-MoM) [16], and the other methods. Both the memory requirement and CPU time are reduced compared with the full three-dimensional methods [17, 19].

In a BOR solution method, the fields and currents are decomposed into different cylindrical harmonic modes. These modes are orthogonal with each other, so they can be solved separately. In a numerical method for BORs, only the generatrix that forms the surface of the BOR is needed to solve the problem. For the scattering and radiation problem from a PEC or homogeneous BOR, it is convenient to use integral equations without the need to use any absorbing boundary condition (ABC). The accuracy is better than the FEM. However, an surface integral equation solver cannot handle an inhomogeneous BOR problem efficiently. The FEM, on the other hand, can perform better for a complex medium [21, 22] and is a good choice especially for inhomogeneous axisymmetric cavity problems with a PEC boundary.

In this work, we extend the higher-order FEM [19, 23] to improve the accuracy for the computation of inhomogeneous axisymmetric cavity problems. Although the higher-order FEM has been applied to 3-D problems, the new contribution of this work is that it develops and applies this method to BOR cavities. Both node- and edge-based elements are used to discretize the azimuthal and meridian components of the field. Numerical results are given to demonstrate the validity and efficiency of the higher-order FEM.

2. FINITE ELEMENT METHOD FOR AXISYMMETRIC RESONATORS

As shown in Figure 1, a BOR is in the cylindrical coordinate system (ρ, ϕ, z), and the medium inside the body is inhomogeneous. Because of the axial symmetry of the geometry, the field inside can be expressed in a Fourier series [1]

$$\mathbf{E}(\rho, \phi, z) = \sum_{m=-\infty}^{\infty} [\mathbf{E}_{t,m}(\rho, z) + \hat{\phi} E_{\phi,m}(\rho, z)] e^{jm\phi} \qquad (1)$$

$$\mathbf{H}(\rho, \phi, z) = \sum_{m=-\infty}^{\infty} [\mathbf{H}_{t,m}(\rho, z) + \hat{\phi} H_{\phi,m}(\rho, z)] e^{jm\phi} \qquad (2)$$

where $\mathbf{E}_{t,m}$, $E_{\phi,m}$, $\mathbf{H}_{t,m}$ and $H_{\phi,m}$ are the electric and magnetic fields in the meridian plane and the azimuthal component of the m-th Fourier mode, respectively. Only a 2-D mesh is needed for analyzing the 3-D
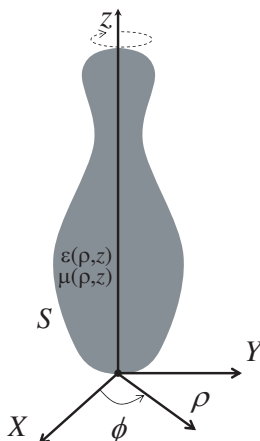
Figure 1. An arbitrary inhomogeneous axisymmetric cavity and the coordinate system.

axisymmetric cavity. As all cylindrical modes are orthogonal to each other, they can be treated separately.

On the axis ($\rho = 0$), the fields must retain the continuity for any values of ϕ [13, 21, 22]. Thus, there are three kinds of conditions for different cylindrical modes: for $m = 0$,

$$E_{\phi,0} = (\nabla \times \mathbf{E})_{\phi,0} = 0 \tag{3}$$

$$E_{\rho,0} = (\nabla \times \mathbf{E})_{\rho,0} = 0 \tag{4}$$

$$E_{z,0} \neq 0, \quad (\nabla \times \mathbf{E})_{z,0} \neq 0 \tag{5}$$

for $m = \pm 1$

$$E_{\rho,\pm 1} = \mp j E_{\phi,\pm 1} \tag{6}$$

$$(\nabla \times \mathbf{E})_{\rho,\pm 1} = \mp j (\nabla \times \mathbf{E})_{\phi,\pm 1} \tag{7}$$

$$E_{z,\pm 1} = (\nabla \times \mathbf{E})_{z,\pm 1} = 0 \tag{8}$$

and for $|m| > 1$

$$E_{\phi,m} = E_{\rho,m} = E_{z,m} = 0 \tag{9}$$

$$(\nabla \times \mathbf{E})_{\phi,m} = (\nabla \times \mathbf{E})_{\rho,m} = (\nabla \times \mathbf{E})_{z,m} = 0 \tag{10}$$

Consider the vector Helmholtz equation for the electric field $\mathbf{E}$

$$-\nabla \times \left(\mu_r^{-1} \nabla \times \mathbf{E} \right) + k_0^2 \epsilon_r \mathbf{E} = j\omega\mu_0 \mathbf{J} + \nabla \times \mu_r^{-1} \mathbf{M} \equiv \mathbf{S}_e \tag{11}$$

where μ_r and ϵ_r are the relative complex permeability and permittivity, respectively. $\mathbf{J}$ and $\mathbf{M}$ are the electric and magnetic current densities, respectively, and k_0 is the wave number in free space. For a source-free

($\mathbf{S}_e = 0$) cavity Ω with a perfect electric conductor outer boundary S, the weak form of the vector wave equation can be expressed as

$$-\int_\Omega (\nabla \times \mathbf{W}_\ell) \cdot (\mu_r^{-1} \nabla \times \mathbf{E}) d\Omega + \int_\Omega k_0^2 \mathbf{W}_\ell \cdot \epsilon_r \mathbf{E} d\Omega = 0 \qquad (12)$$

where $\mathbf{W}_\ell$ is the testing function, and the outer boundary condition

$$\hat{n} \times \mathbf{E}(\mathbf{r}) = 0, \qquad \mathbf{r} \in S \qquad (13)$$

has been utilized, where S is the boundary of the cavity Ω, and $\hat{n}$ is the unit outward normal vector.

In the general 3-D FEM, the basis functions for electromagnetic fields are the mixed-order edge elements. However, for the BOR FEM, when projected onto a meridian cross section, the azimuthal component E_ϕ should use a nodal basis function, while the meridian components $\mathbf{E}_t$ should use a mixed-order edge element. Considering the boundary conditions at $\rho = 0$ for different cylindrical modes as shown in Equations (3)–(10), the m-th cylindrical mode can be expanded as

$$E_{\phi,m} = \sum_{i=1}^{N_n} e_{\phi,i} N_i \qquad (14)$$

$$\mathbf{E}_{t,m} = \delta_{m,0} \sum_{i=1}^{N_s} e_{t,i} \mathbf{N}_i + (1-\delta_{m,0}) \sum_{i=1}^{N_s} e_{t,i} \rho \mathbf{N}_i - (1-\delta_{m,0}) \hat{\rho} \sum_{i=1}^{N_n} e_{\phi,i} \frac{j}{m} N_i (15)$$

where N_n is the number of nodes. N_s is the number of segments (or edges), $e_{\phi,i}$. $e_{t,i}$ are the unknown coefficients. N_i and $\mathbf{N}_i$ represent the standard node-based and edge-based element basis functions, respectively. Note that because of the Kronecker delta function, for $m = 0$ the second and third terms in $\mathbf{E}_{t,m}$ become zero. And the testing function is chosen as:

$$\mathbf{W}_\ell = \left(\sum_{i=1}^{N_n} N_i \hat{\phi} + \sum_{i=1}^{N_s} \mathbf{N}_i \right) e^{j\ell\phi} = W_{\phi,\ell} \hat{\phi} + \mathbf{W}_{t,\ell} \qquad (16)$$

After substituting the basis and testing functions into Equation (12) and making use of the orthogonality of cylindrical modes, the wave equation can be rewritten as

$$2\pi \int_S \frac{\rho}{\mu_r} (\nabla_t \times \mathbf{W}_{t,-m}) \cdot (\nabla_t \times \mathbf{E}_{t,m}) \, dS$$

$$+ 2\pi \int_S \frac{\rho}{\mu_r} \left(\nabla_t W_{\phi,-m} + \frac{jm}{\rho} \mathbf{W}_{t,-m} + \frac{\hat{\rho}}{\rho} W_{\phi,-m} \right)$$

$$\cdot \left(\nabla_t E_{\phi,m} + \frac{-jm}{\rho} \mathbf{E}_{t,m} + \frac{\hat{\rho}}{\rho} E_{\phi,m} \right) dS$$

$$= 2\pi \int_S k_0^2 \epsilon_r \rho \left(\mathbf{W}_{t,-m} \cdot \mathbf{E}_{t,m} + W_{\phi,-m} \cdot E_{\phi,m} \right) dS \qquad (17)$$

a system of equations

$$\begin{bmatrix} K_m^{ee} & K_m^{en} \\ K_m^{ne} & K_m^{nn} \end{bmatrix} \cdot \begin{bmatrix} E^e \\ E^n \end{bmatrix} = k_0^2 \begin{bmatrix} M_m^{ee} & M_m^{en} \\ M_m^{ne} & M_m^{nn} \end{bmatrix} \cdot \begin{bmatrix} E^e \\ E^n \end{bmatrix} \qquad (18)$$

can be formed, where in the stiffness matrix element $K_m^{\alpha\beta}$ and mass matrix element $M_m^{\alpha\beta}$, α and β are the choices for the testing function and the basis function. m is the the mode index. e stands for the edge unknowns. n stands for node-based unknowns. k_0^2 is the eigenvalue of the system, $E^e = (e_{t,1}, e_{t,2}, \cdots, e_{t,N_s})^T$ and $E^n = (e_{\phi,1}, e_{\phi,2}, \cdots, e_{\phi,N_n})^T$. Both the stiffness matrix and mass matrix are sparse. A seven-point numerical integration is used for the impedance matrix assembling. LAPACK routines are used to compute eigenvalues and eigenvectors [18].

3. HIGHER-ORDER FINITE ELEMENT METHOD

In order to improve the accuracy from the conventional FEM with first-order nodal basis functions and first-order edge elements, a higher-order FEM is applied to axisymmetric inhomogeneous dielectric resonators. As shown in Figure 2(a), each triangular element on the meridian plane has three node-based and three edge-based vector basis functions for the conventional lower-order basis functions. The three
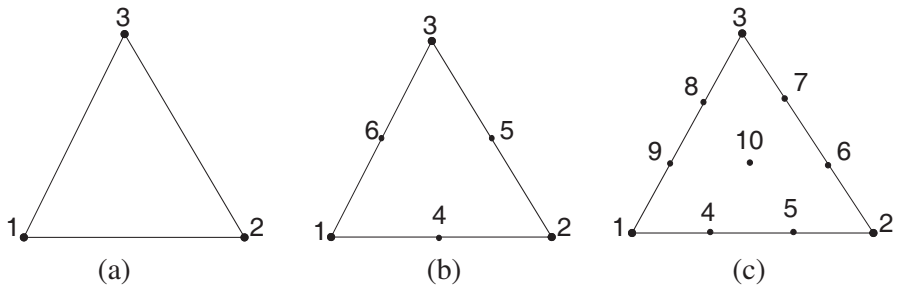
Figure 2. (a) Three-noded triangle for first-order node-based and edge-based basis functions. (b) Six-noded triangle for second-order node-based and edge-based basis functions. (c) Ten-noded triangle for third-order node-based and edge-based basis functions.

nodal basis functions are given by

$$N_i^e = L_i^e, \qquad i = 1, 2, 3 \tag{19}$$

where L_i^e denote the area coordinates for element e, and i is the index of the node. The three edge-based basis functions can be expressed as

$$\mathbf{N}_{ij}^e = l_{ij}^e (L_i^e \nabla L_j^e - L_j^e \nabla L_i^e), \qquad i, j = 1, 2, 3, \ (i \neq j) \tag{20}$$

where l_{ij}^e is the length of the edge from node i to node j. And the vector basis functions have the following properties:

$$\nabla \cdot \mathbf{N}_{ij}^e = 0, \qquad \nabla \times \mathbf{N}_{ij}^e = 2l_{ij}^e \nabla L_i^e \times \nabla L_j^e \tag{21}$$

The second-order node-based and edge-based basis functions are defined on a triangular element with six nodes [19] in Cartesian coordinates and are adapted here to the BOR problem: three of them are corner nodes, and the rest three nodes are mid-side nodes. As shown in Figure 2(b), each element has six nodal basis functions and eight edge-based basis functions. Three of the nodal basis functions are defined on the three corner nodes, while the other three nodal basis functions are defined on the three mid-side nodes. Six of the vector edge-based basis functions are defined at the edges of the triangular element, while the rest two edge-based basis functions are defined inside the triangular element.

The third-order node-based and edge-based basis functions are defined on a triangular element with ten nodes [20] in Cartesian coordinates and are adapted here to the BOR problem: As shown in Figure 2(c), each element has ten nodal basis functions and fifteen edge-based basis functions. Three of the nodal basis functions are defined on the three corner nodes. Six nodal basis functions are defined on the six side nodes, and the last one is defined inside the triangular element. Nine of the vector edge-based basis functions are defined at the edges of the triangular element, while the rest six edge-based basis functions are defined inside the triangular element.

4. NUMERICAL RESULTS

In this section, several numerical results are presented to show the validity of the proposed method.

4.1. An Inhomogeneous BOR Cavity

Lebaric and Kajfez [24] use the finite integration technique to analyze the cavity shown in Figure 3. The mesh of the proposed method contains 307 nodes and 555 triangular elements. Table 1 lists the comparison of the resonant frequencies by measurement and two
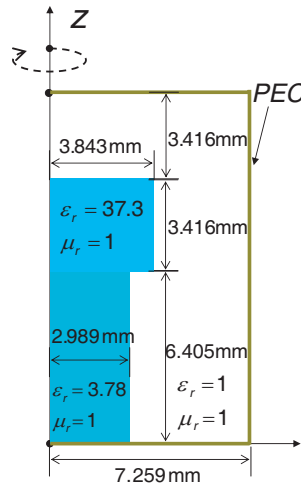
Figure 3. The structure of the cavity investigated by Lebaric and Kajfez [24].

Table 1. Comparison of the resonant frequencies for the cavity investigated by Lebaric and Kajfez [24], and the error of different method with measured data.

Mode	Measured [24] (GHz)	Lebaric [24] (GHz)	Relative Error (%)	This work (GHz)	Relative Error (%)
TE_{01}	6.943	7.037	1.354	7.082	2.002
HEM_{11}	8.694	8.742	0.552	8.847	1.760
HEM_{12}	8.905	8.897	0.090	9.054	1.673
TM_{01}	9.185	9.296	1.208	9.326	1.535
HEM_{21}	10.558	10.605	0.445	10.743	1.752
TM_{02}	10.943	11.113	1.554	11.173	2.102
HEM_{13}	11.184	11.226	0.376	11.471	2.566
TE_{02}	11.316	11.391	0.663	11.668	3.111

numerical methods. The first subscript represents the azimuthal mode m, and the second subscript represents the index for the resonance frequencies for mode m. The relative error is defined by

$$\text{error} = \frac{|f_0 - f_0^{Ref}|_2}{|f_0^{Ref}|_2} \tag{22}$$

where f_0^{Ref} is the measured frequency, and f_0 is the resonance frequency obtained by different numerical methods.

4.2. Convergence of the Higher-order BOR FEM

To study the convergence of the higher-order BOR FEM, a homogeneous PEC cavity filled with air ($\varepsilon_r = 1$, $\mu_r = 1$) is considered. The cavity has a radius $1\,\text{m}$ and a height $1\,\text{m}$. Thus, analytical results can be obtained for this homogeneous cavity to show the accuracy of the higher-order BOR FEM. The error in the numerical solution is defined in the L_2-norm as

$$\text{error} = \frac{\left| k_0^{BOR} - k_0^{Ref} \right|_2}{\left| k_0^{Ref} \right|_2} \tag{23}$$

where k_0^{Ref} is the reference result (here obtained analytically), and k_0^{BOR} is the result by the BOR FEM implemented in this work. Figures 4–5 show the relative error of the eigenvalue for different modes (TM_{m11}, $m = 0, 2$) versus the sampling density (SD) in terms of the number of points per wavelength (PPW) defined as

$$\text{SD} = \lambda_{\min} \sqrt{\frac{(N_n + N_s)}{2S}} \quad \text{(PPW)} \tag{24}$$
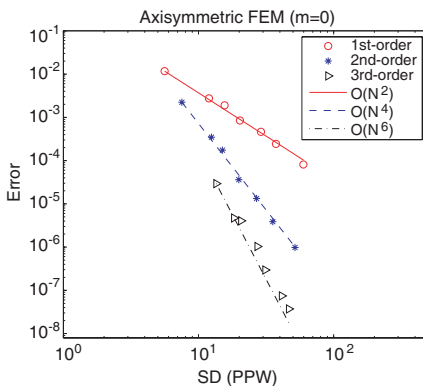
Figure 4. Relative error of the eigenvalue (3.956360747459228) of the axisymmetric cavity for cylindrical mode TM_{011} versus the SD.
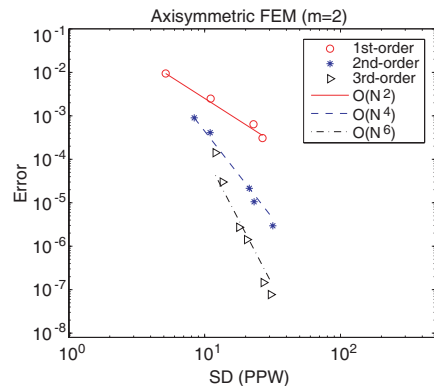
Figure 5. Relative error of the eigenvalue (6.020317336175292) of the axisymmetric cavity for cylindrical mode TM_{211} versus the SD.

where S is the area of the meridian cross section, and $\lambda_{\min}$ is the wavelength corresponding to the first eigenvalue. Numerical results show that the first-order FEM has second-order accuracy. The second-order FEM has forth-order accuracy, and the third-order FEM has sixth-order accuracy for all of the modes ($m = 0, \pm 1, \pm 2, \ldots$). Figure 6
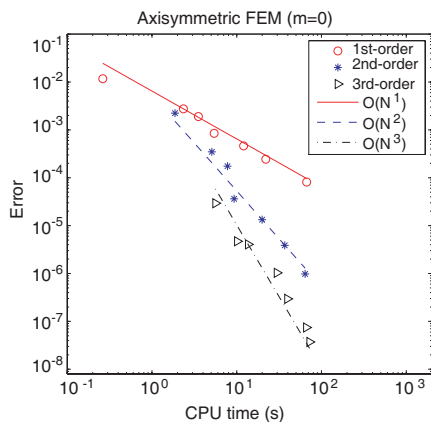
Figure 6. Relative error of the eigenvalue (3.956360747459228) of the axisymmetric cavity for cylindrical mode TM_{011} versus the CPU time.
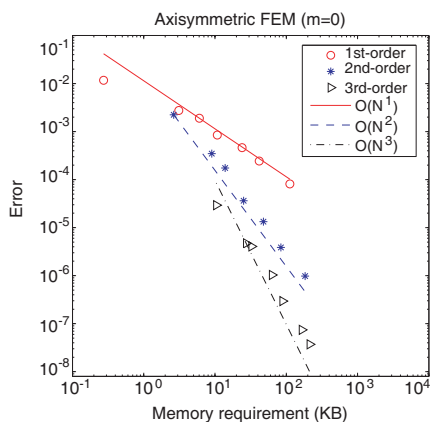
Figure 7. Relative error of the eigenvalue (3.956360747459228) of the axisymmetric cavity for cylindrical mode TM_{011} versus the memory requirement for the impedance matrix.
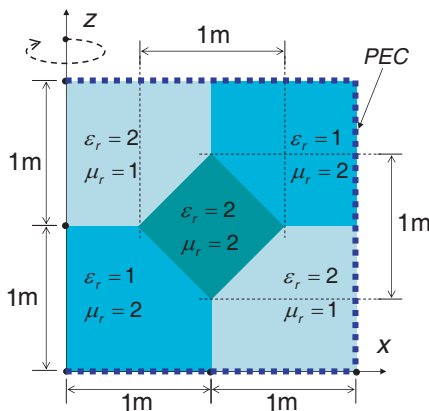
Figure 8. The meridian cross section of the complex axisymmetric cavity.

shows the relative error of the eigenvalue for the mode (TM_{011}) versus the CPU time. Figure 7 shows the relative error of the eigenvalue for the mode (TM_{011}) versus the memory requirement for assembling the impedance matrix. It is observed that with higher-order FEM, both CPU time and memory requirement are significantly reduced from the low-order FEM for given accuracy.

Table 2. The eigenvalue k_0 (m^{-1}) of the complex inhomogeneous BOR resonator in Fig. 8 for cylindrical modes $m = 0$, 1, and 2.

$m = 0$ TM	$m = 0$ TE	$m = 1$	$m = 2$
0.758319467983	1.556665293282	1.100060683411	1.409270983878
1.385410832002	2.310095127483	1.367848384402	1.719496785904
1.845430933757	2.531857231466	1.715618353533	2.072418330069
2.187346916473	3.078603247897	1.955593596103	2.261525441642
2.241053842087	3.309581132676	2.159744765452	2.373896486525
2.767949199031	3.438014224975	2.343318049667	2.658461907026
2.885644692555	3.903209914022	2.459948977338	2.772251939479
3.156606620535	3.994776034044	2.669140591017	3.004470924506
3.269750790287	4.166803722899	2.735047784798	3.098721511754
3.570998532440	4.485704821550	2.906014517201	3.223265931716
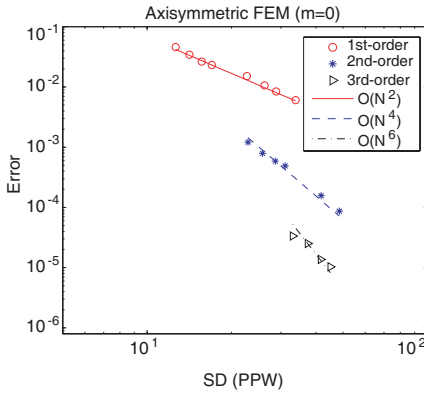
Figure 9. Relative error of the eigenvalue (2.310095127483) of the complex axisymmetric cavity for the cylindrical mode $m = 0$ versus the SD.
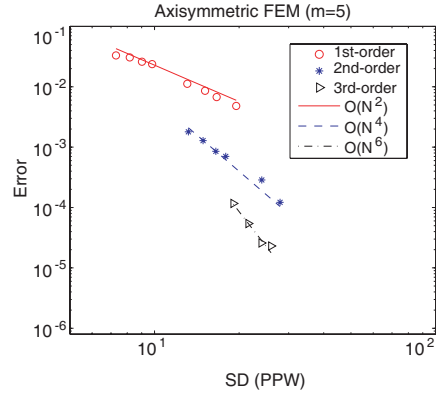
Figure 10. Relative error of the eigenvalue (4.007018370180) of the complex axisymmetric cavity for the cylindrical mode $m = 5$ versus the SD.

Table 3. The eigenvalue k_0 (m^{-1}) of the complex inhomogeneous BOR resonator in Fig. 8 for cylindrical modes $m = 3, 4, 5$.

$m = 3$	$m = 4$	$m = 5$
1.741288135988	2.089327786115	2.446968521519
2.088713198590	2.470310589431	2.858386128340
2.448982140927	2.828224973396	3.127842596151
2.542311359568	2.836539544915	3.224016571322
2.655823101522	2.971791478477	3.311348574190
2.927621205386	3.222956968676	3.543834017584
3.147832453686	3.502013629732	3.847975677459
3.289801576308	3.596876181138	3.918241508939
3.460509874489	3.727092908436	4.007018370180
3.526869035357	3.893109485341	4.204014602936

4.3. A Complex Inhomogeneous Cavity

As shown in Figure 8, a complex axisymmetric cavity filled with an inhomogeneous medium is simulated by the BOR FEM with different orders. The cavity is filled with three different types of dielectric materials as shown in the figure. The third-order FEM result with a sampling density of 30 PPW ($N_n = 1147$, $N_s = 2610$) is set as the reference result, as listed in Tables 2–3.

Figures 9–10 show the relative error for different modes. The third-order FEM has the highest accuracy. The order of accuracy for the eigenvalues is 2, 4, and 6 for the first-, second-, and third-order BOR FEM.

5. CONCLUSION

In this paper, a higher-order FEM is applied to solve the eigenvalue problem for arbitrary inhomogeneous dielectric axisymmetric resonators. The proposed method uses higher-order node-based elements for the azimuthal field component and higher-order edge-based elements for the meridian field components. It has been observed that the higher-order mixed basis functions can significantly improve the accuracy with the same number of unknowns when compared with a lower-order FEM. Furthermore, for given accuracy, higher-order FEM can significantly reduce the memory requirement and CPU time compared with a lower-order FEM.

REFERENCES

1. Andreasen, M. G., "Scattering from bodies of revolution," *IEEE Trans. Antennas Propag.*, Vol. 13, 303–310, Mar. 1965.

2. Mautz, J. R. and R. F. Harrington, "Radiation and scattering from bodies of revolution," *Appl. Sci. Res.*, Vol. 20, 405–435, Jun. 1969.

3. Wu, T. K. and L. L. Tsai, "Scattering from arbitrarily-shaped lossy dielectric bodies of revolution," *Radio Sci.*, Vol. 12, 709–718, Sep.–Oct. 1977.

4. Medgyesi-Mitschg, L. N. and J. M. Putnam, "Electromagnetic scattering from axially inhomogeneous bodies of revolution," *IEEE Trans. Antennas Propag.*, Vol. 32, 797–806, Aug. 1984.

5. Huddleston, P. L., L. N. Medgyesi-Mitschg, and J. M. Putnam, "Combined field integral equation formulation for scattering by dielectrically coated conducting bodies," *IEEE Trans. Antennas Propag.*, Vol. 34, 510–520, Apr. 1986.

6. Liu, Q. H. and W. C. Chew, "Diffraction of nonaxisymmetric waves in cylindrically layered media by horizontal discontinuities," *Radio Sci.*, Vol. 27, No. 5, 569–581, 1992.

7. Liu, Q. H., "Electromagnetic field generated by an off-axis source in a cylindrically layered medium with an arbitrary number of horizontal discontinuities," *Geophysics*, Vol. 58, No. 5, 616–625, 1993.

8. Cao, X.-Y. and J. Gao, "The singularity problem at the wire/surface junction region for antenna and arrays with bodies of revolution," *Progress In Electromagnetics Research B*, Vol. 10, 117–130, 2008.

9. Rui, X., J. Hu, and Q. H. Liu, "Fast inhomogeneous plane wave algorithm for homogeneous dielectric body of revolution," *Commun. Comput. Phys.*, accepted.

10. Qiu, Z. and C. M. Butler, "Analysis of a wire in the presence of an open body of revolution," *Progress In Electromagnetics Research*, PIER 15, 1–26, 1997.

11. Abdelmageed, A. K., "Efficient evaluation of modal Green's functions arising in EM scattering by bodies of revolution," *Progress In Electromagnetics Research*, PIER 27, 337–356, 2000.

12. Lee, J. F., G. Wilkins, and R. Mittra, "Finite-element analysis of axisymmetric cavity resonator using a hybrid edge element technique," *IEEE Trans. Microwave Theory Tech.*, Vol. 41, 1981–1987, 1993.

13. Wong, M. F., M. Park, and V. Frouad Hanna, "Axisymmetric edge-based finite element formulation for bodies of revolution: Application to dielectric resonators," *IEEE Microwave Symp. MTT-S*, Orlando, FL, 1995.

14. Richalot, E., M. F. Wong, V. Frouad Hanna, and H. Naudrand, "Analysis of radiating axisymmetric structures using a 2-D finite-element and spherical mode expansion," *Microwave Opt. Technol. Lett.*, Vol. 20, 8–13, 1999.

15. Hoppe, D. J., L. W. Epp, and J. F. Lee, "A hybrid symmetric FEM/MOM formulation applied to scattering by inhomogeneous bodies of revolution," *IEEE Trans. Antennas Propag.*, Vol. 42, 798–805, Jun. 1994.

16. Moneum, M. A. A., Z. Shen, J. L. Volakis, and O. Graham, "Hybrid PO-MoM analysis of large axi-symmetric radomes," *IEEE Trans. Antennas Propag.*, Vol. 49, 1657–1666, Dec. 2001.

17. Rao, S. M., D. R. Wilton, and A. W. Glission, "Electromagnetic scattering by surfaces of arbitrary shape," *IEEE Trans. Antennas Propag.*, Vol. 30, 409–418, 1982.

18. Anderson, E., Z. Bai, C. Bischof, S. Blackford, J. Demmel, J. Dongarra, J. Du Croz, A. Greenbaum, S. Hammarling, A. McKenney, and D. Sorensen, *LAPACK User's Guide*, 3rd Edition, SIAM, Philadelphia, 1999.

19. Jin, J. M., *The Finite Element Method in Electromagnetics*, John Wiley & Sons, New York, 1993.

20. Peterson, A. F., S. L. Ray, and R. Mittra, *Computational Methods for Electromagnetics*, IEEE Press, 1998.

21. Greenwood, A. D. and J. M. Jin, "A novel efficient algorithm for scattering from a complex BOR using mixed finite elements and cylindrical PML," *IEEE Trans. Antennas Propag.*, Vol. 47, 620–629, 1999.

22. Greenwood, A. D. and J. M. Jin, "Finite-element analysis of complex axisymmetric radiating structures," *IEEE Trans. Antennas Propag.*, Vol. 47, 1260–1266, 1999.

23. Savage, J. S. and A. F. Peterson, "Higher order vector finite elements for tetrahedral cells," *IEEE Trans. Microwave Theory Tech.*, Vol. 44, 874–879, 1996.

24. Lebaric, J. E. and D. Kajfez, "Analysis of dielectric resonator cavities using the finite integration technique," *IEEE Trans. Microwave Theory Tech.*, Vol. 37, 1740–1748, 1989.